Numerical modeling of non-Newtonian viscoplastic flows: Part II. Viscoplastic fluids and general tridimensional topographies

Noé Bernabeu, Pierre Saramito, Claude Smutek

INTERNATIONAL JOURNAL OF
NUMERICAL ANALYSIS AND MODELING
Volume 1, Number 1, Pages 1–18

NUMERICAL MODELING OF NON-NEWTONIAN VISCOPLASTIC FLOWS: PART II. VISCOPLASTIC FLUIDS AND GENERAL TRIDIMENSIONAL TOPOGRAPHIES

NOÉ BERNABEU[1,2], PIERRE SARAMITO[1], AND CLAUDE SMUTEK[2]

(Communicated by Yanping Lin)

Abstract. A new reduced model for the shallow tridimensional viscoplastic fluid is presented in this paper, allowing for the first time an arbitrarily topography. A new numerical approach is also proposed in order to catch efficiently the long-time behavior of the flow and the arrested state. In order to support varying and large time steps, a fully implicit and second order method (BDF2) is proposed. It is combined with an auto-adaptive mesh feature for catching accurately the evolution of front position. This approach was tested on two flows experiments and compared to experimental measurements. The first study shows the efficiency of this approach when the shallow flow conditions are fully satisfied while the second one points out the limitations of the reduced model when these conditions are not fulfilled.

Key words. fluid mechanics ; non-Newtonian fluid ; Bingham model ; asymptotic analysis ; shallow water theory

1. Introduction

The study of shallow flows is motivated by numerous environmental and industrial applications. For Newtonian fluids, this problem was first motivated by hydraulic engineering applications. In 1887, Barré de Saint-Venant [30] introduced for fast Newtonian flows the shallow water approximation, driven by inertia terms while viscous effects are neglected. The original technique, based on an averaged flow-depth, has been extended to the more general asymptotic expansion method. It leads to the same governing equation at zeroth expansion order, but provides a more general theoretical framework for the derivation of reduced models. More recently, slower Newtonian flows [19] and the effect of viscous terms [13] were investigated. But only the more complex non-Newtonian case approaches the complexity of both the manufacturing processes (concretes, foods) and the environmental applications (e.g. mud flows [12, 21], volcanic lava [14, 36], dense snow avalanches [2] or submarine landslides [15]). Concerning non-Newtonian rheologies, shallow approximations of the dam break problem were first studied for a viscoplastic fluid by Lui and Mei [22] and revisited by Balmforth and Craster [6]. See [8, 3] for recent reviews on this subject and [1] for some recent theoretical avances. One may also note the recent interest for the Bostwick consistometer used in food industry [28, 7]. The 2D horizontal dam break problem was used as a benchmark test: the nonlinear reduced equation obtained by the asymptotic method in the shallow limit does not admit an explicit solution and composite [18] or autosimilar solutions [17, 5] were proposed instead (see also [4]).

Thus, a direct numerical resolution without any simplification is of the utmost interest to fully solve such a nonlinear problem. Let us mention the computation

Received by the editors October 6, 2012 and, in revised form, June 25, 2013.
2000 *Mathematics Subject Classification.* 35K65, 65M50, 65M60, 76A05.

of the arrested state [24] by a specific finite difference scheme. Nevertheless, the proposed numerical procedure is based on some specific features of the solution of the horizontal 1D dam break problem and does not extend to a more general situation, such as non-constant slopes or 3D topographies. Some authors explored specific 3D topographies by using specific axisymmetric coordinate systems such as a curved channel [25] or a conical surface [37]. These authors used a finite difference discretization scheme and then, an alternating direction algorithm for solving the resulting algebraic nonlinear set of equations. This numerical approach was next reused in [8] for similar 3D computations on a flat inclined topography. It is important to note that all previous reduced models was developed for some specific topography and not reusable for another one.

The aim of this paper is to bring a new robust and efficient numerical method for the resolution of the shallow approximation of 3D viscoplastic flow problem on a general topography. Numerical results obtained with the present model are validated by comparisons with previous computations on specific topographies. The proposed numerical algorithm for solving the problem extends a previous numerical work preformed on the horizontal 2D dam break problem [35]. The present numerical scheme provides a fully automatic space-adaptive feature which enables an accurate capture of the evolution of front position and which is also able to predict accurately the long-time behavior and the arrested state of the model.

This manuscript has been divided as follow: Section 2 introduces the problem statement and the reduced problem obtained after the asymptotic analysis under the shallow flow approximation. Section 3 develops details of the numerical resolution of this nonlinear problem. Section 4 presents the numerical results and two comparisons between the present theory and experiment measurements available in the literature.

2. The reduced problem for a general 3d topography

2.1. Problem statement. The Herschel-Bulkley [16] constitutive equation expresses the deviatoric part τ of the stress tensor versus the rate of deformation tensor $\dot\gamma$ as:

$$\left\{\begin{array}{ll} \tau = K|\dot\gamma|^{n-1}\dot\gamma + \tau_y \frac{\dot\gamma}{|\dot\gamma|} & \text{when } \dot\gamma \neq 0, \\ |\tau| \leq \tau_y & \text{otherwise.} \end{array}\right. \tag{1}$$

where $K > 0$ is the consistency, $n > 0$ is the power-law index and τ_y is the yield stress. Here $|\tau| = ((1/2)\sum_{i,j=1}^{3} \tau_{ij}^2)^{1/2}$ denotes the conventional norm of a symmetric tensor in mechanics. The total Cauchy stress tensor is $\sigma = -p.I + \tau$ where p is the pressure and I the identity tensor. When $n = 1$ and $\tau_y = 0$, the fluid is Newtonian and K is the viscosity. For a general $n > 1$ and when $\tau_y = 0$, the model describes a power-law fluid. When $n = 1$ and $\tau_y \geq 0$, this model reduces to the Bingham one [9]. The constitutive equation (1) is completed by the conservations of momentum and mass:

$$\rho\left(\partial_t \mathbf{u} + \mathbf{u}\cdot\nabla\mathbf{u}\right) - \mathbf{div}(-p.I + \tau) = \rho\mathbf{g}, \tag{2}$$

$$\operatorname{div}\mathbf{u} = 0, \tag{3}$$

where $\rho > 0$ is the constant density and $\mathbf{g}$ is the gravity vector. There are three equations (1)-(3) and three unknowns τ, $\mathbf{u}$ and p. The corresponding problem is closed by defining the boundary and initial conditions.

The flow over a variable topography is considered (see Fig. 1). For any time $t > 0$, the flow domain is denoted as $Q(t)$. We suppose that $Q(t)$ can be described

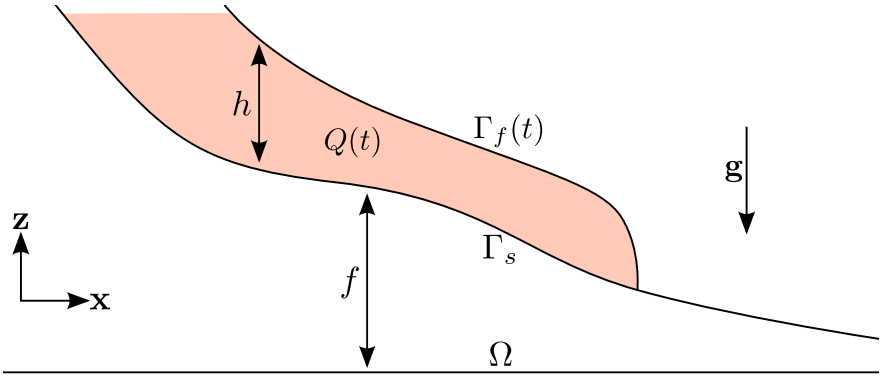

FIGURE 1. Schematic view of a flow on a variable topography.

as:

$$Q(t) = \{(x, y, z) \in \Omega \times \mathbb{R};\ f(x, y) < z < f(x, y) + h(t, x, y)\}$$

where Ω is an open and bounded subset of $\mathbb{R}^2$. Here, f denotes the topography and h the flow height. The boundary $\partial Q(t)$ splits in three parts: the bottom relief Γ_s, the top free surface $\Gamma_f(t)$, and the lateral part $\Gamma_w(t)$, defined by:

$$\begin{aligned} \Gamma_s &= \{(x, y, z) \in \Omega \times \mathbb{R};\ z = f(x, y)\} \\ \Gamma_f(t) &= \{(x, y, z) \in \Omega \times \mathbb{R};\ z = f(x, y) + h(t, x, y)\} \\ \Gamma_w(t) &= \{(x, y, z) \in \partial\Omega \times \mathbb{R};\ f(x, y) < z < f(x, y) + h(t, x, y)\} \end{aligned}$$

For any $t > 0$, the boundary conditions expresses the non-slip condition on the bottom and lateral boundaries and the null stress on the free surface:

$$\mathbf{u} = 0 \text{ on } \Gamma_s \cup \Gamma_w(t) \tag{4}$$

$$\sigma \cdot \boldsymbol{\nu} = 0 \text{ on } \Gamma_f(t) \tag{5}$$

where $\boldsymbol{\nu}$ is the unit outward normal on $\partial Q(t)$. It remains to describe the evolution of the free surface. It is convenient to introduce the level set function φ that expresses as:

$$\varphi(t, x, y, z) = z - f(x, y) - h(t, x, y).$$

Note that the zero level set, where $\varphi(t, x, y, z) = 0$, is exactly the free surface. The level set function is transported by the flow: $\partial_t \varphi + \mathbf{u} \cdot \nabla \varphi = 0$,. On $\Gamma_s(t)$, where $z = f + h$, this writes:

$$\partial_t h + u_x \partial_x (f + h) + u_y \partial_y (f + h) - u_z = 0,\ \forall t > 0 \text{ and } (x, y) \in \Omega. \tag{6}$$

This transport equation for the height h is completed by an initial condition:

$$h(t = 0, x, y) = h_{init}(x, y),\ \forall (x, y) \in \Omega. \tag{7}$$

where h_{init} is given. The set of equation is finally completed by an initial condition for the velocity $\mathbf{u}$:

$$\mathbf{u}(t = 0) = \mathbf{u}_{init} \text{ in } Q(0) \tag{8}$$

The problem expresses as: find h, τ, $\mathbf{u}$ and p satisfying (1)-(8).

2.2. Dimensional analysis.

2.2.1. The dimensionless procedure. In this paragraph, the asymptotic analysis, introduced by Lui and Mei [22] and revisited by Balmforth and Craster [6] for a bidimensional flow on a constant slope, is here extended to the case of tridimensional flow on a arbitrarilly topography. Let H be a characteristic length of the bidimensional domain Ω and H a characteristic height of the flow. We introduce the dimensionless parameter $\varepsilon = H/L$. Let $U = \rho g H^3/(\eta L)$ be a characteristic flow velocity in the (x, y) plane, where $\eta = K\,(U/H)^{n-1}$ is a representative viscosity and $g = |\mathbf{g}|$ is the gravity constant. Replacing this expression of η, we obtain:

$$U = \left(\frac{\rho g H^2}{KL}\right)^{\frac{1}{n}} H$$

Let $W = \varepsilon U$ be a characteristic velocity in the z direction, $T = L/U$ a characteristic time, and $P = \rho g H$ a characteristic pressure. The problem is reformulated with dimensionless quantities and unknowns, denoted with tildes:

$$x = L\tilde{x}, y = L\tilde{y}, z = H\tilde{z}, t = T\tilde{t}, p = P\tilde{p}, h = H\tilde{h},$$
$$u_x = U\tilde{u}_x, u_y = U\tilde{u}_y, u_z = \varepsilon U\tilde{u}_z.$$

Notice the non-isotropic scaling procedure for the z coordinate and the z vector component of the velocity vector $\mathbf{u}$. The dimensionless rate of deformation tensor $\tilde{\dot{\gamma}}$ is also related to its dimensional counterpart $\dot{\gamma} = \nabla\mathbf{u} + \nabla\mathbf{u}^T$ by the following non-isotropic relations:

$$\begin{aligned}
\dot{\gamma}_{\alpha\beta} &= (U/L)\,\tilde{\dot{\gamma}}_{\alpha\beta}, \quad \alpha,\beta \in \{x,y\} \\
\dot{\gamma}_{\alpha z} &= (U/H)\,\tilde{\dot{\gamma}}_{\alpha z}, \quad \alpha \in \{x,y\} \\
\dot{\gamma}_{zz} &= (U/L)\,\tilde{\dot{\gamma}}_{zz}.
\end{aligned}$$

The scalling procedure for the deviatoric part of stress τ is similar:

$$\begin{aligned}
\tau_{\alpha\beta} &= \eta\,(U/L)\,\tilde{\tau}_{\alpha\beta}, \quad \alpha,\beta \in \{x,y\}, \\
\tau_{\alpha z} &= \eta\,(U/H)\,\tilde{\tau}_{\alpha z}, \quad \alpha \in \{x,y\}, \\
\tau_{zz} &= \eta\,(U/L)\,\tilde{\tau}_{zz}.
\end{aligned}$$

2.2.2. The constitutive equation. The dimensionless rate of deformation tensor can be expressed versus the dimensionless velocity as:

$$\begin{aligned}
\tilde{\dot{\gamma}}_{\alpha\beta} &= \partial_{\tilde{\beta}}\tilde{u}_\alpha + \partial_{\tilde{\alpha}}\tilde{u}_\beta, \quad \alpha,\beta \in \{x,y\}, \\
\tilde{\dot{\gamma}}_{\alpha z} &= \partial_{\tilde{z}}\tilde{u}_\alpha + \varepsilon^2\partial_{\tilde{\alpha}}\tilde{u}_z, \quad \alpha \in \{x,y\}, \\
\tilde{\dot{\gamma}}_{zz} &= 2\partial_{\tilde{z}}\tilde{u}_z.
\end{aligned}$$

The tensor norm scales as: $|\dot{\gamma}| = (U/L)\,|\tilde{\dot{\gamma}}|$. Using (3), we get: $|\tilde{\dot{\gamma}}| = \varepsilon^{-1}E$ where

$$\begin{aligned}
E = \big\{&\varepsilon^2(\partial_{\tilde{x}}\tilde{u}_y + \partial_{\tilde{y}}\tilde{u}_x)^2 + 2\varepsilon^2(\partial_{\tilde{x}}\tilde{u}_x)^2 + 2\varepsilon^2(\partial_{\tilde{y}}\tilde{u}_y)^2 \\
&+2\varepsilon^2(\partial_{\tilde{x}}\tilde{u}_x + \partial_{\tilde{y}}\tilde{u}_y)^2 + (\partial_{\tilde{z}}\tilde{u}_x + \varepsilon^2\partial_{\tilde{x}}\tilde{u}_z)^2 + (\partial_{\tilde{z}}\tilde{u}_y + \varepsilon^2\partial_{\tilde{y}}\tilde{u}_z)^2\big\}^{\frac{1}{2}}
\end{aligned}$$

Let us introduce the Bingham dimensionless number Bi that compares the yield stress τ_y to a characteristic viscous stress $\eta U/H$:

$$Bi = \frac{\tau_y H}{\eta U} = \varepsilon^{-1}\frac{\tau_y}{\rho g H}.$$

We suppose that $Bi = \mathcal{O}(1)$ in ε. This hypothesis interprets as $\tau_y/(\rho g H) = \mathcal{O}(\varepsilon)$ or equivalently that the yield stress τ_y is supposed to be small when compared to

the gravity effets $\rho g H$. When $|\tau| \geq \tau_y$ we obtain a dimensionless version of the constitutive equation (1):

$$\tilde{\tau}_{ij} = \left(\frac{Bi}{E} + E^{n-1} \right) \tilde{\dot{\gamma}}_{ij}$$

Then $|\tau| = \eta(U/L)|\tilde{\tau}|$ where $|\tilde{\tau}| = \varepsilon^{-1} T$ and

$$T = \left\{ \tilde{\tau}_{xz}^2 + \tilde{\tau}_{yz}^2 + \frac{1}{2}\varepsilon^2 \tilde{\tau}_{xx}^2 + \frac{1}{2}\varepsilon^2 \tilde{\tau}_{yy}^2 + \frac{1}{2}\varepsilon^2 \tilde{\tau}_{zz}^2 + \varepsilon^2 \tilde{\tau}_{xy}^2 \right\}^{\frac{1}{2}}.$$

Remark that the von Mises condition $|\tau| \geq \tau_y$ then becomes $T \geq Bi$. The constitutive equation (1) writes:

$$\left\{ \begin{array}{ll} \tilde{\tau} = \left[\frac{Bi}{E} + E^{n-1} \right] \tilde{\dot{\gamma}}_{ij} & \text{when } E \neq 0, \\ T < Bi & \text{otherwise.} \end{array} \right. \tag{9}$$

2.2.3. The conservation laws. Let us introduce the Reynolds number:

$$Re = \frac{\rho U L}{\eta} = \frac{\rho^2 g H^3}{\eta^2}.$$

We suppose that $Re = \mathcal{O}(1)$ in ε. It means that the flow is supposed to be sufficiently slow for the inertia effects to be neglected at the zeroth order of development in ε. The conservation of momentum and mass (2)-(3) become:

$$\begin{aligned}
\varepsilon^2 Re(\partial_{\tilde{t}} \tilde{u}_x + \tilde{u}_x \partial_{\tilde{x}} \tilde{u}_x + \tilde{u}_y \partial_{\tilde{y}} \tilde{u}_x + \tilde{u}_z \partial_{\tilde{z}} \tilde{u}_x) &= -\partial_{\tilde{x}} \tilde{p} + \varepsilon^2 (\partial_{\tilde{x}} \tilde{\tau}_{xx} + \partial_{\tilde{y}} \tilde{\tau}_{xy}) + \partial_{\tilde{z}} \tilde{\tau}_{xz}, && \text{(10a)} \\
\varepsilon^2 Re(\partial_{\tilde{t}} \tilde{u}_y + \tilde{u}_x \partial_{\tilde{x}} \tilde{u}_y + \tilde{u}_y \partial_{\tilde{y}} \tilde{u}_y + \tilde{u}_z \partial_{\tilde{z}} \tilde{u}_y) &= -\partial_{\tilde{y}} \tilde{p} + \varepsilon^2 (\partial_{\tilde{x}} \tilde{\tau}_{xy} + \partial_{\tilde{y}} \tilde{\tau}_{yy}) + \partial_{\tilde{z}} \tilde{\tau}_{yz}, && \text{(10b)} \\
\varepsilon^4 Re(\partial_{\tilde{t}} \tilde{u}_z + \tilde{u}_x \partial_{\tilde{x}} \tilde{u}_z + \tilde{u}_y \partial_{\tilde{y}} \tilde{u}_z + \tilde{u}_z \partial_{\tilde{z}} \tilde{u}_z) &= -\partial_{\tilde{z}} \tilde{p} + \varepsilon^2 (\partial_{\tilde{x}} \tilde{\tau}_{xz} + \partial_{\tilde{y}} \tilde{\tau}_{yz} + \partial_{\tilde{z}} \tilde{\tau}_{zz}) - 1, && \text{(10c)} \\
\partial_{\tilde{x}} \tilde{u}_x + \partial_{\tilde{y}} \tilde{u}_y + \partial_{\tilde{z}} \tilde{u}_z &= 0. && \text{(10d)}
\end{aligned}$$

2.2.4. Boundary and initial conditions. The non-slip boundary condition (4) on $\Gamma_s \cup \Gamma_w$ writes:

$$\tilde{\mathbf{u}} = 0$$

The unit outward normal $\boldsymbol{\nu}$ on the free surface $\Gamma_s(t)$ expresses as:

$$\boldsymbol{\nu} = \frac{\nabla \varphi}{||\nabla \varphi||} = \frac{1}{\sqrt{1 + |\nabla(f+h)|^2}} \begin{pmatrix} -\partial_x(f+h) \\ -\partial_y(f+h) \\ 1 \end{pmatrix}.$$

Then (5) writes:

$$\begin{pmatrix} \tau_{xx} - p & \tau_{xy} & \tau_{xz} \\ \tau_{xy} & \tau_{yy} - p & \tau_{yz} \\ \tau_{xz} & \tau_{yz} & \tau_{zz} - p \end{pmatrix} \begin{pmatrix} -\partial_x(f+h) \\ -\partial_y(f+h) \\ 1 \end{pmatrix} = \begin{pmatrix} 0 \\ 0 \\ 0 \end{pmatrix}.$$

and becomes in dimensionless form:

$$\begin{aligned}
-(\varepsilon^2 \tilde{\tau}_{xx} - \tilde{p}) \partial_{\tilde{x}} (\tilde{f} + \tilde{h}) - \varepsilon^2 \tilde{\tau}_{xy} \partial_{\tilde{y}} (\tilde{f} + \tilde{h}) + \tilde{\tau}_{xz} &= 0 && \text{(11a)} \\
-\varepsilon^2 \tilde{\tau}_{xy} \partial_{\tilde{x}} (\tilde{f} + \tilde{h}) - (\varepsilon^2 \tilde{\tau}_{yy} - \tilde{p}) \partial_{\tilde{y}} (\tilde{f} + \tilde{h}) + \tilde{\tau}_{yz} &= 0 && \text{(11b)} \\
-\varepsilon^2 \tilde{\tau}_{xz} \partial_{\tilde{x}} (\tilde{f} + \tilde{h}) - \varepsilon^2 \tilde{\tau}_{yz} \partial_{\tilde{y}} (\tilde{f} + \tilde{h}) + \varepsilon^2 \tilde{\tau}_{zz} - \tilde{p} &= 0 && \text{(11c)}
\end{aligned}$$

where $\tilde{f} = f/H$ denotes the dimensionless topography and is known. The transport equation (6) for the flow height h becomes:

$$\partial_{\tilde{t}} \tilde{h} + \tilde{u}_x \partial_{\tilde{x}} (\tilde{f} + \tilde{h}) + \tilde{u}_y \partial_{\tilde{y}} (\tilde{f} + \tilde{h}) - \tilde{u}_z = 0. \tag{12}$$

The dimensionless problem is completed by the initial conditions for the dimensionless height and velocity. The initial (1)-(7) problem and its dimensionless version are equivalent, since the change of unknowns is simply linear.

2.3. The reduced problem.

2.3.1. The zeroth order problem. In this paragraph, we only consider the dimensionless problem: since there is no ambiguity, we omit the tilde on the dimensionless variables. We assume that the unknown admit the following development in ε when $\varepsilon \ll 1$:

$$\begin{aligned} \tau &= \tau_0 + \varepsilon\tau_1 + \varepsilon^2\tau_2 + \dots \\ \mathbf{u} &= \mathbf{u}_0 + \varepsilon\mathbf{u}_1 + \varepsilon^2\mathbf{u}_2 + \dots \\ p &= p_0 + \varepsilon p_1 + \varepsilon^2 p_2 + \dots \\ h &= h_0 + \varepsilon h_1 + \varepsilon^2 h_2 + \dots \end{aligned}$$

In this paragraph, we aim at obtaining the problem at the zero order for τ_0, $\mathbf{u}$, p_0 and h_0. Since we only consider the zeroth order, we also omit the zero subscript in this paragraph. Let us denote $\nabla_{||} = (\partial_x, \partial_y)$ the gradient vector in the $0xy$ plane, $\mathbf{u}_{||} = (u_x, u_y)$ the projected velocity in this plane and $\boldsymbol{\tau}_{||} = (\tau_{xz}, \tau_{yz})$ the shear stress vector in the same plane. For any $\mathbf{v}_{||} = (v_x, v_y)$ we also denote as $\mathrm{div}_{||}\mathbf{v}_{||} = \partial_x v_x + \partial_y v_y$ the corresponding plane divergence and $\left|\mathbf{v}_{||}\right| = (v_x^2 + v_y^2)^{1/2}$ the usual Euclidean norm in $\mathbb{R}^2$. For convenience, we also denote as $\mathbf{dir}(\mathbf{v}_{||}) = \mathbf{v}_{||}/\left|\mathbf{v}_{||}\right|$ the direction of any nonzero plane vector. With these notations, we have $E = \left|\partial_z \mathbf{u}_{||}\right|$ and $T = \left|\boldsymbol{\tau}_{||}\right|$ at the zeroth order. The constitutive equation (9) then reduces to:

$$\tau_{\alpha z} = \left[\frac{Bi}{\left|\partial_z \mathbf{u}_{||}\right|} + \left|\partial_z \mathbf{u}_{||}\right|^{n-1}\right] \partial_z u_\alpha, \quad \forall \alpha \in \{x, y\}, \tag{13a}$$

$$\tau_{\alpha\beta} = \left[\frac{Bi}{\left|\partial_z \mathbf{u}_{||}\right|} + \left|\partial_z \mathbf{u}_{||}\right|^{n-1}\right] (\partial_\beta u_\alpha + \partial_\alpha u_\beta), \quad \forall \alpha, \beta \in \{x, y\}, \tag{13b}$$

$$\tau_{zz} = 2\left[\frac{Bi}{\left|\partial_z \mathbf{u}_{||}\right|} + \left|\partial_z \mathbf{u}_{||}\right|^{n-1}\right] \partial_z u_z, \tag{13c}$$

when $\nabla\mathbf{u} + \nabla\mathbf{u}^T \neq 0$ and

$$\left|\boldsymbol{\tau}_{||}\right| \leq Bi, \quad \text{otherwise.} \tag{13d}$$

From the conservation laws (10) we get at the zeroth order:

$$\partial_z \tau_{xz} - \partial_x p = 0, \tag{14a}$$

$$\partial_z \tau_{yz} - \partial_y p = 0, \tag{14b}$$

$$-\partial_z p = -1, \tag{14c}$$

$$\partial_x u_x + \partial_y u_y + \partial_z u_z = 0. \tag{14d}$$

The free surface boundary condition (11) at $z = f(x, y) + h(t, x, y)$ reduces at the zeroth order to:

$$\tau_{xz} + p\partial_x(f + h) = 0, \tag{15a}$$

$$\tau_{yz} + p\partial_y(f + h) = 0, \tag{15b}$$

$$p = 0. \tag{15c}$$

The others equations, i.e. the transport equation (12), the non-slip boundary condition and the initial conditions for $\mathbf{u}$ and h, are unchanged at the zeroth order.

2.3.2. Reducing the problem. In this paragraph, we show that the zeroth order problem reduces to a nonlinear parabolic problem with h as the only unknown: all the others quantities τ, $\mathbf{u}$ and p at the zeroth order can be computed from h by an explicit expression.

From (15) we get at the free surface $z = f + h$:

$$p(z{=}f+h) = 0, \tag{16a}$$

$$\boldsymbol{\tau}_{||}(z{=}f+h) = 0. \tag{16b}$$

Integrating (14c) in z from $z = 0$ to $z = f + h$ and using (16a), we have:

$$p(t,x,y,z) = f(x,y) + h(t,x,y) - z. \tag{17}$$

As f is known, the quantity p depends only of the unknown h. From (15a)-(15b), we then obtain an explicit expression for the shear stress:

$$\boldsymbol{\tau}_{||} = -(f+h-z)\nabla_{||}(f+h). \tag{18}$$

Remark that $\boldsymbol{\tau}_{||}$ is linear in z: since there exists a $z \in [f, f+h]$ where $\left|\boldsymbol{\tau}_{||}\right| \geq Bi$ and, from (16b), $\left|\boldsymbol{\tau}_{||}\right| = 0$ at $z = f + h$, there exists an intermediate height $h_c(t,x,y) \in [0, h(t,x,y)]$ for which $|\boldsymbol{\tau}_{||}(z{=}f+h_c)| = Bi$ and we have:

$$h_c(t,x,y) = \max\left(0, h - \frac{Bi}{|\nabla_{||}(f+h)|}\right). \tag{19}$$

The von Mises criteria at the zeroth order writes equivalently as:

$$\left|\boldsymbol{\tau}_{||}\right| > Bi \iff (f+h-z)|\nabla_{||}(f+h)| > Bi \iff z \in [f, f+h_c[$$

Taking the Euclidean norm of (13a) leads to

$$|\boldsymbol{\tau}_{||}| = Bi + |\partial_z \mathbf{u}_{||}|^n. \tag{20}$$

Then from (18) and (20), we get:

$$\left|\partial_z \mathbf{u}_{||}\right| = \begin{cases} \left|\nabla_{||}(f+h)\right|^{\frac{1}{n}} \ (f+h_c-z)^{\frac{1}{n}} & \text{when } z \in [f, f+h_c] \\ 0 & \text{when } z \in \,]f+h_c, f+h] \end{cases}$$

Taking the direction of (13a) leads to $\mathbf{dir}(\boldsymbol{\tau}_{||}) = \mathbf{dir}(\partial_z \mathbf{u}_{||}) = -\mathbf{dir}(\nabla_{||}(f+h))$ and then:

$$\partial_z \mathbf{u}_{||} = \begin{cases} -\left|\nabla_{||}(f+h)\right|^{\frac{1}{n}} \ (f+h_c-z)^{\frac{1}{n}} \ \mathbf{dir}(\nabla_{||}(f+h)) & \text{when } z \in [f, f+h_c] \\ 0 & \text{when } z \in \,]f+h_c, f+h] \end{cases}$$

In the zeroth order problem, the $z = f(x,y) + h_c(t,x,y)$ surface splits the flow in two zones: the $z \leq f + h_c$ zone is sheared while the $z \geq f + h_c$ one is rigid. Remark that when $h_c = 0$, i.e. when $\left|h\,\nabla_{||}(f+h)\right| < Bi$, there is only a rigid zone. Thanks to the non-slip boundary condition at $z = f$, the fluid is locally arrested. After summation from $z = f$ to $z = f + h_c$, and using the non-slip boundary condition $\mathbf{u}_{||} = 0$ at $z = f$ and the continuity of $\mathbf{u}_{||}$ at $z = f + h_c$, we get:

$$\mathbf{u}_{||} = \begin{cases} \frac{n}{n+1}\left|\nabla_{||}(f+h)\right|^{\frac{1}{n}} \ \mathbf{dir}(\nabla_{||}(f+h)) \ \left[(f+h_c-z)^{\frac{n+1}{n}} - h_c{}^{\frac{n+1}{n}}\right] \\ \qquad\qquad \text{when } z \in [f, f+h_c] \\ -\frac{n}{n+1}\left|\nabla_{||}(f+h)\right|^{\frac{1}{n}} \ \mathbf{dir}(\nabla_{||}(f+h)) \ h_c{}^{\frac{n+1}{n}} \\ \qquad\qquad \text{when } z \in \,]f+h_c, f+h] \end{cases} \tag{21}$$

The last component of the velocity is obtained by integrating the mass conservation (10d) in $[f, z]$:

$$\int_f^z \partial_x u_x \mathrm{d}z + \int_f^z \partial_y u_y \mathrm{d}z + \int_f^z \partial_z u_z \mathrm{d}z = 0 \tag{22}$$

From the non-slip boundary condition, $u_z = 0$ at $z = f$, we get:

$$u_z(t, x, y, z) = -\int_{f(x,y)}^z \mathrm{div}_{||}(\mathbf{u}_{||})\, \mathrm{d}z \tag{23}$$

Thus, velocity $\mathbf{u}$ admits an explicit expression depending only upon h. Then, the complete stress τ follows explicitly from (13).

It remains to obtain a characterization of h alone. Let us consider (23) at $z = f+h$: by swapping the derivation ∂_x and ∂_y with the integral over $[f(x, y), f(x, y)+h(t, x, y)]$, and using the non-slip boundary condition at $z = f$, we get:

$$\int_f^{f+h} \partial_\alpha u_\alpha \mathrm{d}z = \partial_\alpha \left(\int_f^{f+h} u_\alpha \mathrm{d}z \right) - u_\alpha(t, x, y, f + h)\partial_\alpha(f + h), \ \forall \alpha \in \{x, y\}$$

Combining the previous relation with the transport equation (12) at the zeroth order, and replacing in (23) at $z = f + h$, leads to:

$$\partial_t h + \mathrm{div}_{||} \left(\int_f^{f+h} \mathbf{u}_{||} \mathrm{d}z \right) = 0$$

By replacing in the previous equation $\mathbf{u}_{||}$ by its expression (21), depending only upon h, we obtain, after rearrangements, the following conservative equation for h:

$$\partial_t h - \mathrm{div}_{||} \left\{ \mu_n \left(Bi,\, h,\, \left| \nabla_{||}(f + h) \right| \right) \ \nabla_{||}(f + h) \right\} = 0 \ \text{ in }]0, +\infty[\times\Omega \tag{24}$$

Here, μ_n denotes a diffusion coefficient, defined for all $n > 1$ and all $Bi, h, \xi \in \mathbb{R}^+$ by:

$$\mu_n(Bi,\, h,\, \xi) = \begin{cases} \dfrac{n\ ((n+1)h\xi + nBi)\ (h\xi - Bi)^{1+\frac{1}{n}}}{(n+1)\ (2n+1)\ \xi^3} & \text{when } h\xi > Bi, \\ 0 & \text{otherwise.} \end{cases} \tag{25}$$

This expression contains the two parameters n and Bi of the Herschel-Bulkley viscoplastic fluid. The non-slip velocity condition at the lateral boundaries leads to an homogeneous Neumann boundary condition:

$$\frac{\partial(f + h)}{\partial n} = 0 \text{ on }]0, +\infty[\times\partial\Omega \tag{26}$$

where $\partial/\partial n = \mathbf{n}.\nabla_{||}$ and $\mathbf{n}$ denotes the outward unit normal on $\partial\Omega$ in the Oxy plane. Recall the initial condition:

$$h(t=0) = h_{init} \text{ in } \Omega \tag{27}$$

The reduced problem writes: find $h(t, x, y)$, defined for all $t > 0$ and $(x, y) \in \Omega$ and satisfying (24), (26) and (27).

Notice that, for a Newtonian flow ($n = 1$ and $Bi = 0$), expression (25) simplifies as:

$$\mu_1(0, h, \xi) = \frac{h^3}{3}$$

For a power-law fluid ($n > 0$ and $Bi = 0$):

$$\mu_n(0, h, \xi) = \begin{cases} \dfrac{n\ h^{2+\frac{1}{n}}}{(2n+1)\ \xi^{1-\frac{1}{n}}} & \text{when } \xi \neq 0, \\ 0 & \text{otherwise.} \end{cases}$$

For the Bingham model ($n = 1$ and $Bi \geq 0$):

$$\mu_1(Bi, h, \xi) = \begin{cases} \dfrac{(2h\xi + Bi)\ (h\xi - Bi)^2}{6\ \xi^3} & \text{when } h\xi > Bi, \\ 0 & \text{otherwise.} \end{cases}$$

2.3.3. A new dimensionless formulation. Going back to dimensional variable, the zeroth order equation (26) writes:

$$\partial_t h - \left(\frac{\rho g}{K}\right)^{\frac{1}{n}}\ \mathrm{div}_{||}\left\{\mu_n\left(\frac{\tau_y}{\rho g},\, h,\, \left|\nabla_{||}(f+h)\right|\right)\ \nabla_{||}(f+h)\right\} \quad = \quad 0$$

From a computational point of view, it is convenient to consider a new dimensionless formulation. This second dimensionless procedure differs from the previous one as ε does no more appears in the zeroth order problem: the new dimensionless quantities are denoted with an hat. Let H be a characteristic length of the problem and let:

$$\hat{h} = \frac{h}{H},\ \hat{x} = \frac{x}{H},\ \hat{y} = \frac{y}{H},\ \hat{t} = \frac{t}{T},\ \hat{f} = \frac{f}{H},$$

where $T = \left(\frac{K}{\rho g H}\right)^{\frac{1}{n}}$ represents a characteristic time. After variable substitution, we obtain the following zeroth order dimensionless equation:

$$\partial_{\hat{t}}\hat{h} - \hat{\mathrm{div}}_{||}\left\{\mu_n\left(\widehat{Bi},\, \hat{h},\, \left|\hat{\nabla}_{||}(\hat{f}+\hat{h})\right|\right)\ \hat{\nabla}_{||}(\hat{f}+\hat{h})\right\} \quad = \quad 0$$

where $\widehat{Bi} = \tau_y/(\rho g H)$ is the Bingham number related to this new dimensionless procedure. As we now only consider this dimensionless problem, and since there is no ambiguity, we omit the hat for all the quantities and also for the Bingham number.

3. Numerical method

The nonlinear parabolic problem is first discretized in time by a full implicit second order variable step scheme (BFD2) and then, the resulting subproblems are discretized in space by an adaptive quadratic finite element method.

3.1. Second order implicit scheme. Let $(t_m)_{m\geq 0}$ the discrete times and $\Delta t_m = t_{m+1} - t_m,\ m \geq 0$ the corresponding time steps. As the observed solutions decrease exponentially to an arrested state, we choose a geometric progression for the time step $\Delta t_{m+1} = \theta \Delta t_m$ where $\theta > 1$ and Δt_0 are given.

The time derivative is approximated by the following backward second order variable step finite difference scheme (BFD2), defined for all $\varphi \in C^0$ by:

$$\frac{\partial \varphi}{\partial t}(t_{m+1}) = \frac{2\Delta t_m + \Delta t_{m-1}}{\Delta t_m(\Delta t_m + \Delta t_{m-1})}\varphi(t_{m+1}) - \frac{\Delta t_m + \Delta t_{m-1}}{\Delta t_m \Delta t_{m-1}}\varphi(t_m)$$
$$+ \frac{\Delta t_m}{(\Delta t_m + \Delta t_{m-1})\Delta t_{m-1}}\varphi(t_{m-1}) + \mathcal{O}(\Delta t_m^2 + \Delta t_{m-1}^2).$$

The approximate solution sequence $(h_m)_{m\geq 0}$, $h_m \approx h(m\Delta t)$, is defined recursively, for all $m \geq 1$ by:

$(P)_m$: h^{m-1} and h^m being known, find h^{m+1} such that:

$$\alpha_m h^{m+1} - \mathrm{div}_{||}\left\{\mu_n\left(Bi,\, h^{m+1},\, \left|\nabla_{||}(f+h^{m+1})\right|\right)\nabla_{||}(f+h^{m+1})\right\} = g_m \ \text{ in } \Omega \tag{28a}$$

$$\frac{\partial(f+h^{m+1})}{\partial n} = 0 \ \text{ on } \partial\Omega \tag{28b}$$

where

$$\alpha_m = \frac{2\Delta t_m + \Delta t_{m-1}}{\Delta t_m(\Delta t_m + \Delta t_{m-1})}$$

$$g_m = \frac{\Delta t_m + \Delta t_{m-1}}{\Delta t_m \Delta t_{m-1}} h^m - \frac{\Delta t_m}{(\Delta t_m + \Delta t_{m-1})\Delta t_{m-1}} h^{m-1}$$

The sequence is initiated by $h^{-1} = h^0 = h_{init}$ for $m = -1$ and 0, respectively. The initial time-dependent nonlinear parabolic problem is transformed as a sequence of nonlinear subproblem (28) in h^{m+1}. An under-relaxed fixed point algorithm is used for solving these subproblems. The sequence $(\varphi_k)_{k\geq 0}$ of the fixed point iteration is initiated with $\varphi^0 = h^m$ for $k = 0$. Then, for $k \geq 0$, φ^k being known, a prediction φ^* is computed as the solution of the following linear subproblem:

$$\alpha_m\varphi^* - \mathrm{div}_{||}\left\{\mu_n\left(Bi,\, \varphi^k,\, \left|\nabla(f+\varphi^k)\right|\right)\nabla_{||}\varphi^*\right\} = g_m + \mathrm{div}(\mu_n\{\varphi^k, |\nabla(f+\varphi^k)|\}\nabla f) \ \text{ in } \Omega$$

$$\frac{\partial(f+\varphi^*)}{\partial \mathbf{n}} = 0 \ \text{ on } \partial\Omega$$

Finally, φ^{k+1} is defined by the following under-relaxed scheme:

$$\varphi^{k+1} = \omega\varphi^* + (1-\omega)\varphi^k$$

The relaxation parameter $0 < \omega \leq 1$ aims at improving the convergence properties of the sequence, while the unrelaxed case is obtained with $\omega = 1$. The stopping criteria of the fixed point algorithm is defined by the residue of the nonlinear subproblem that should be less than a given tolerance. At convergence, we set $h^{m+1} \leftarrow \varphi^{k+1}$. The choice of ω depends upon n, the power-law index of the fluid rheology (see also [33] for a similar analysis on the p-Laplacian nonlinear problem). We observe that when $n < 1$ and decreases, then ω should be chosen smaller for the algorithm to converge efficiently. The linear subproblem (29) is completely standard and is efficiently solved by a quadratic finite element method, as provided by the [33] library.

3.2. Auto-adaptive mesh procedure. In order to improve both the accuracy and the computing time of the previous algorithm, we use an anisotropic auto-adaptive mesh procedure. Such a procedure was first introduced in [34] for viscoplastic Bingham flows and then extended in [29], and we refer to these articles for implementation details. The procedure bases on a mesh adaptation loop at each time step: the goal is to catch accurately the evolution of the front of the free surface, were $h = 0$ and the associated gradient is sharp (see Fig. 2). As the time approximation is a second order one, the adaptation criterion c takes into account the also solution at two previous time steps: $c = h_{m+1} + h_m + h_{m-1}$.

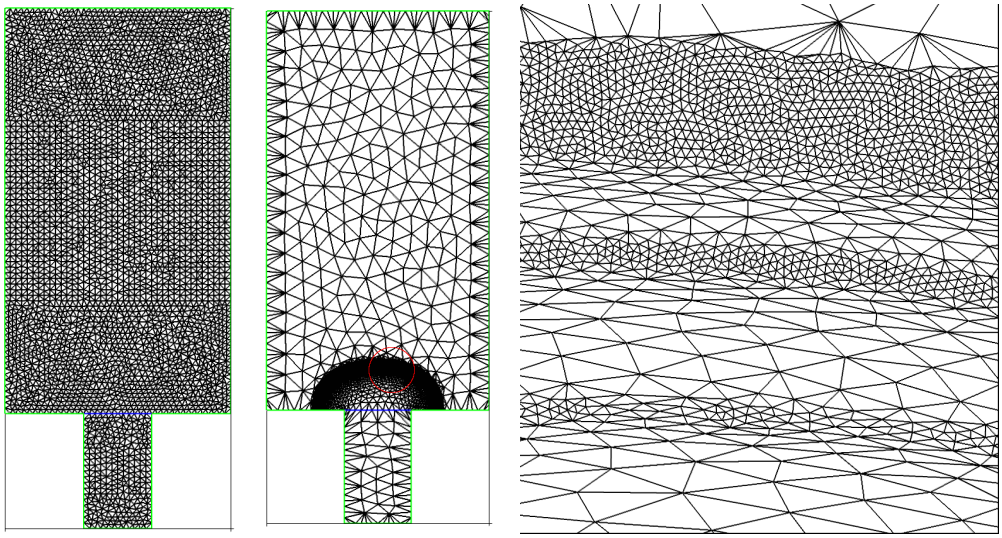

FIGURE 2. Uniform (left) and dynamic auto-adaptive meshes (center). Zoom near the front (right).

4. Comparison with experiments

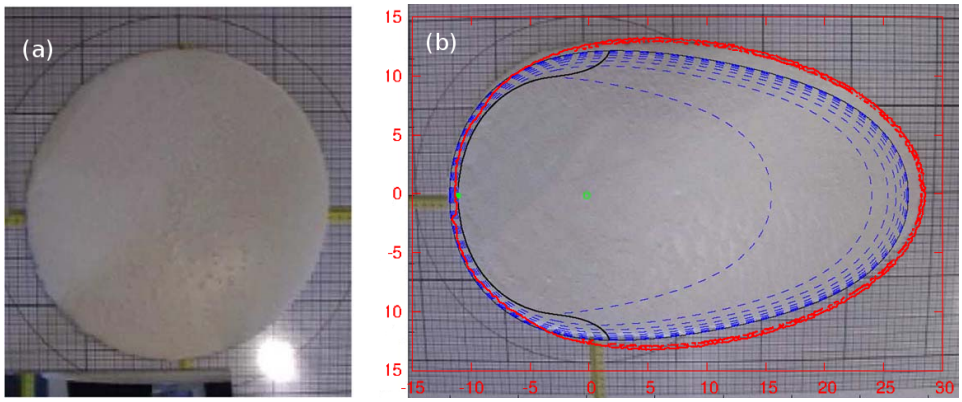

FIGURE 3. The kaolin experiment with $\alpha = 9.6°$: (a) initial state and (b) final one. Comparison of the final front position between experiments from [8] in black and present computations in red. Successive computed front position from [8] are in blue.

4.1. Comparison with the Balmforth et *al.* experiment. The experiment is described in Balmforth et *al* [8]. It bases on kaolin suspension initially at the rest on an horizontal plane, as a dome (see Fig. 3.a). The initial dome diameter is $L = 0.32$ m and its height is $H = 0.016$ m. At $t = 0$, the plane is inclined to a predefined angle α. A first experiment is performed with $\alpha = 9.6°$ and a second one with $\alpha = 3.4°$. The kaolin is characterized by a density $\rho = 1600$ kg.m^{-3}, a power-law index $n = 0.5$, a consistence $K = 40$ Pa.s^{-n}, and a yield stress $\tau_y = 13.4$ Pa. The dimensionless numbers are $\varepsilon = H/L = 5\,10^{-2}$, $Bi = \tau_y/(\rho g H) \approx 5.3\,10^{-2}$, and $Re \approx 6.3\,10^{-3}$. Thus, the hypothesis made on these dimensionless numbers during the asymptotic analysis are here fully validated.

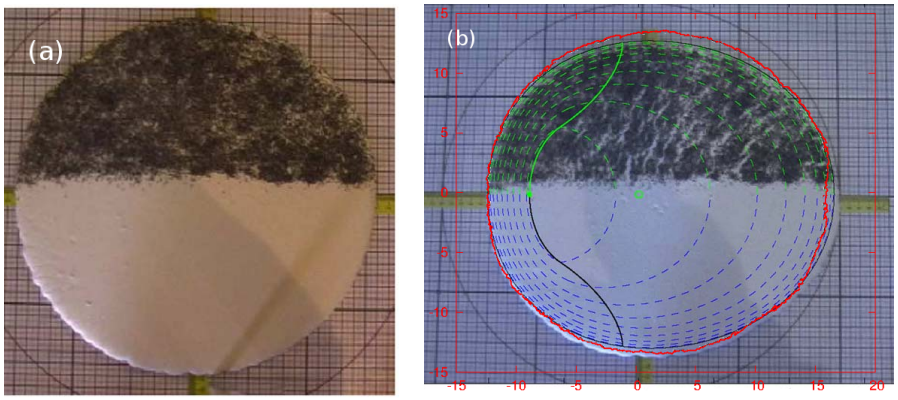

FIGURE 4. The kaolin experiment with $\alpha = 3.4°$: (a) initial state and (b) final one. Comparison of the arrested front position between experiments from [8] in black and present computations in red. Successive computed front position from [8] are in blue.

Fig. 3.b shows the final state: the red line draws the front position of the final solution, as computed by the present method while blue lines are the successive front positions, as computed by Balmforth et *al* [8]. Observe the good correspondence between the two computations and the experiment. Fig. 4 shows a similar comparison for the smaller slope $\alpha = 3.4°$. Also these numerical results were in good concordance with those obtained by [8] and following a numerical algorithm proposed in [25].

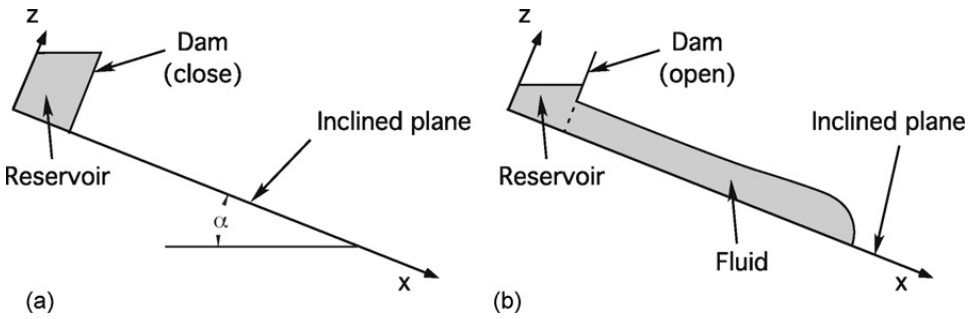

FIGURE 5. Schematic view of the Cochard and Ancey 3D dam break experiment [11].

4.2. Comparison with the Cochard and Ancey experiment. The 3D dam break experiments of Cochard and Ancey [11] is simulated here by the present numerical method. The fluid is initially in a reservoir: at $t = 0$ the dam is opened and the fluid flows on a $\alpha = 12°$ slope. The reservoir has $L = 0.51$ m length and 0.30 m width, and the initial flow height varies from $H = 0.30$ m to 0.36 m in the inclined reservoir (see Fig. 5). The experiment was performed with a 0.30% Carbopol Ultrez 10 solution which is mainly a viscoplastic fluid. The fluid density is $\rho = 811$ kg.m^{-3}, the power-law index $n = 0.415 \pm 0.021$, the consistency $K = 47.7 \pm 1.7$ Pa.s^{-n} and the yield stress $\tau_y = 89 \pm 1$ Pa. The dimensionless numbers are $\varepsilon = 0.59$, $Bi = \dfrac{\tau_y}{\rho g H} \approx 0.037$ and $Re = 1.2\,10^6$. Observe that ε is not so small and that Re is not negligible. This experimental set is expected to test the limitations of the present method.

Fig. 6 plots in the left column the experimental visualization performed by [11] for various times and the corresponding numerical simulations, as obtained by the present method, are represented in the right column. Observe first that, in the experimental apparatus, the door does not disappear instantaneously: its takes about 0.19 s for the door to be completely open. In the numerical simulations of the dam-break problem, the whole bulk of fluid was assumed to be released instantaneously, i.e. the time needed for the gate to open was neglected. Nevertheless, observe the good qualitative correspondence of the flow until the complete arrested state. A more quantitative comparison is shown on Fig. 7: the successive front positions are compared with experimental observations. The agreement is now less favorable: the numerical prediction of the front is characterized by a longer spreading and a smaller advance. There are several possible explanations for these discrepancies. First, the hypothesis made by the asymptotic expansion are not valid in this case, as $\varepsilon = 0.59$ is not so small. Second, the Reynolds number is not negligible, at least during the first seconds, when the inertia effects are no more negligible and that 3D effects develops at the vicinity of the dam. In that case, our asymptotic analysis is no more valid. Third, the experimental delay to open the dam induces some discrepancies. Finally the carbopol is not strictly a viscoplastic fluid: it also develops viscoelastic properties [27, 23] that are not taken into account in the present computations. A more complete model, that extends Herschel-Bulkley one to viscoelastic effects [31, 32] should be considered, and then a new reduced model derived. Let us mention that Nikitin et *al.* [26] recently performed a numerical simulation of the same experiment by another approach, based on a tridimensional approximation of the viscoplastic Herschel-Bulkley by a regularized model. While tridimensional

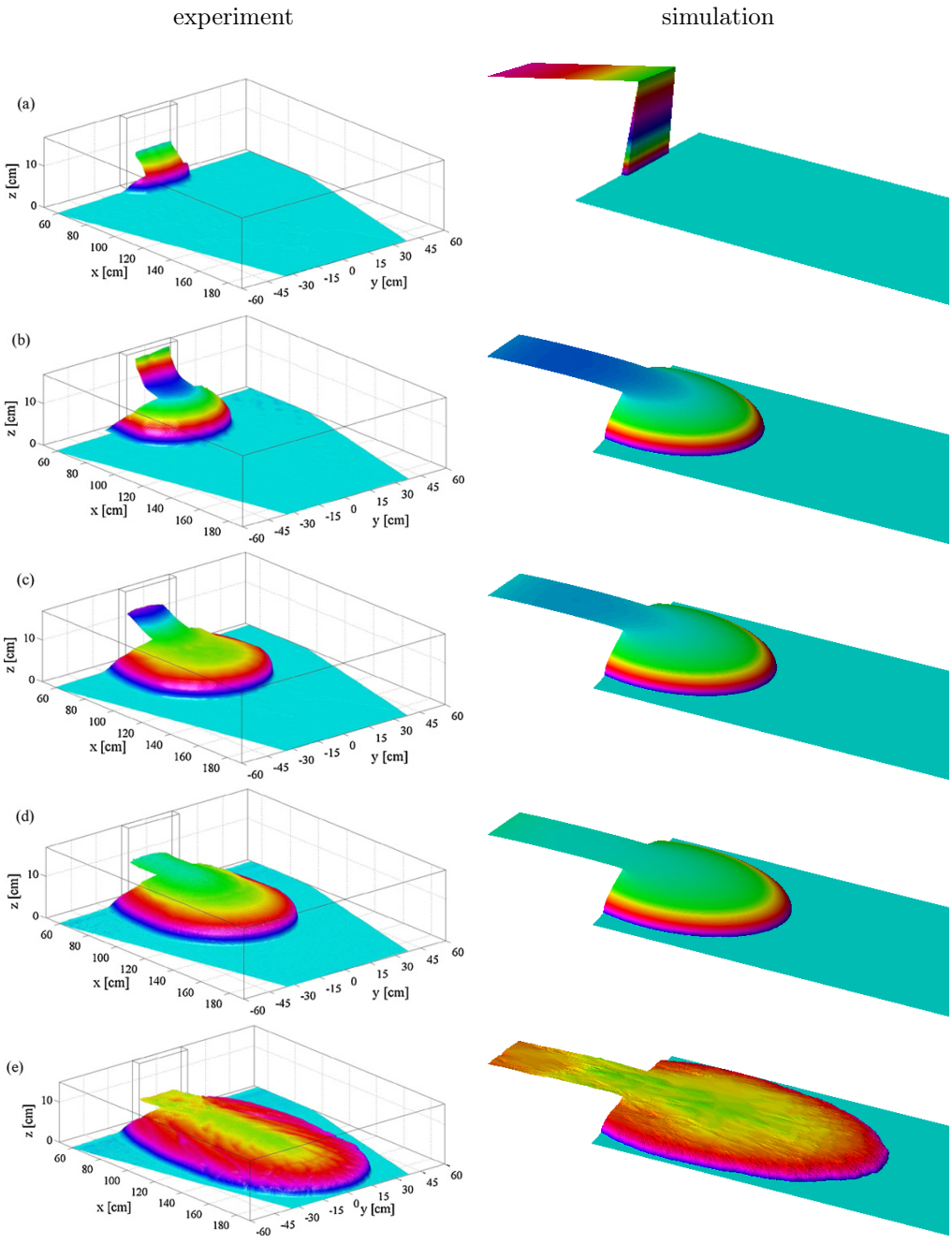

FIGURE 6. The carbopol experiment: left: experimental visualization [11]; right: present numerical simulation. (a) $t = 0$ s, (b) $t = 0.3$ s, (c) $t = 0.6$ s, (d) $t = 1.4$ s et (e) $t = 52$ min.

effects are taken into account for the first time in such simulations, the comparisons are not validated by comparisons with the experimental data of the front position and a possible arrested state is not treated. For shallow models, the arrested state is asymptotically reached [24] For the full model, without free surface and also without

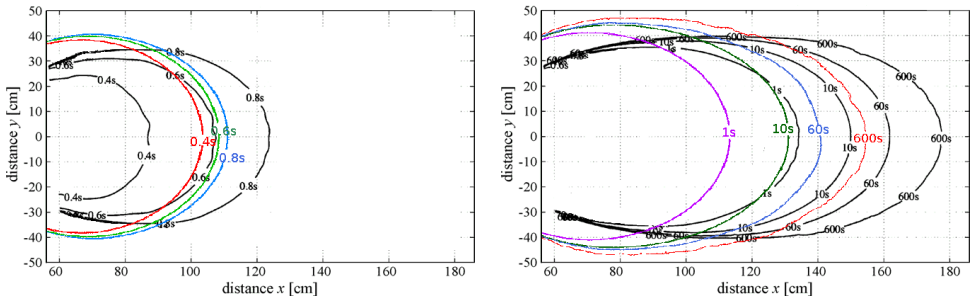

FIGURE 7. The carbopol experiment: comparison of the successive front position. Experiments from [11] are in black and present computations with colors.

the shallow flow approximation, Chatzimina et al. [10] showed that, for the particular Poiseuille or Couette flows, the ideal viscoplastic flow reaches complete cessation at a finite time, while the regularized flow reaches a flow regime corresponding to a small but nonzero flow rate. Thus, the regularization procedure could be a trouble in such viscoplastic time-dependent computations. Also without free surfaces [20, p. 183] showed that the stationary solution of the 3D general viscoplastic models is zero (or a solid motion) under some general conditions. This blocking property is closely related to the limit load analysis, i.e. when the yield stress is sufficiently large or the load forces sufficiently small. While there is nothing to your knowledge about the existence of an arrested state for free surface tridimensional model, it is a reasonable assumption that corresponds to experimental observations.

5. Conclusion

A new reduced model for the shallow tridimensional viscoplastic fluid flowing on a general topography was presented in this paper. In order to catch efficiently both the front position and the long time behavior, an implicit second order time-dependent numerical algorithm was proposed, combined with an auto-adaptive mesh. This approach was tested on two flows experiments and compared to experimental measurements. The first study shows the efficiency of this approach when the shallow flow conditions are fully satisfied: the prediction of the model are in agreement with experimental results. Numerical simulation was also in agreement with a previous computation [8] available for this first test. Computations in [8] are based on a semi-implicit alternating direction method. As the method is only semi-implicit, arbitrarily large time steps are not allowed and the algorithm proposed in [8] is expected to require more computations than the present one for capturing the long time behavior. The second test case points out the limitations of the reduced model when shallow flow conditions are not fully satisfied: the predicted arrested state slightly differs with the experimental observation. A fully 3D simulation, based on a regularized Bingham model was also available for this second test. Nevertheless, this fully 3D computation was not able to reach the arrested state: it could be due to the use of a regularized version of the Bingham model, while the reduced model presented in this paper bases on a sharp (un-regularized) one. Future works will focus on applications to volcanic lava flows and temperature-dependent problems.

References

[1] C. Acary-Robert, E. Fernández-Nieto, G. Narbona-Reina, and P. Vigneaux. A well-balanced finite volume-augmented Lagrangian method for an integrated Herschel-Bulkley model. *J. Sci. Comput.*, 53 (2012) 608–641.

[2] C. Ancey. *Snow avalanches*, pages 319–338. Springer, 2001.

[3] C. Ancey. Plasticity and geophysical flows: a review. *J. Non-Newtonian Fluid Mech.*, 142 (2007) 4–35.

[4] C. Ancey and S. Cochard. The dam-break problem for Herschel-Bulkley viscoplastic fluids down steep flumes. *J. Non-Newtonian Fluid Mech.*, 158 (2009) 18–35.

[5] C. Ancey, S. Cochard, and N. Andreini. The dam-break problem for viscous fluids in the high-capillary-number limit. *J. Fluid Mech.*, 624 (2009) 1–22.

[6] N. J. Balmforth and R. V. Craster. A consistent thin-layer theory for Bingham plastics. *J. Non-Newtonian Fluid Mech.*, 84 (1999) 65–81.

[7] N. J. Balmforth, R. V. Craster, P. Perona, A. C. Rust, and R. Sassi. Viscoplastic dam breaks and the Bostwick consistometer. *J. Non-Newtonian Fluid Mech.*, 142 (2007) 63–78.

[8] N. J. Balmforth, R. V. Craster, A. C. Rust, and R. Sassi. Viscoplastic flow over an inclined surface. *J. Non-Newtonian Fluid Mech.*, 139 (2006) 103–127.

[9] E. C. Bingham. *Fluidity and plasticity*. Mc Graw-Hill, New-York, USA, 1922.

[10] M. Chatzimina, G. C. Georgiou, E. Mitsoulis, and R. R. Huilgol. Cessation of Couette and Poiseuille flows of a Bingham plastic and finite stopping times. *J. Non-Newtonian fluid mechn.*, 129 (2005) 117–127.

[11] S. Cochard and C. Ancey. Experimental investigation of the spreading of viscoplastic fluids on inclined planes. *J. Non-Newtonian Fluid Mech.*, 158 (2009) 73–84.

[12] P. Coussot. Steady, laminar, flow of concentrated mud suspensions in open channel. *J. Hydr. Res.*, 32 (1994) 535–559.

[13] J.-F. Gerbeau and B. Perthame. Derivation of viscous Saint-Venant system for laminar shallow water; numerical validation. *Discrete and continuous dynamical systems - serie B*, 1 (2001) 89–102.

[14] R. W. Griffiths. The dynamics of lava flows. *Annual Review of Fluid Mechanics*, 32 (2000) 477–518.

[15] M. A. Hampton, H. J. Lee, and J. Locat. Submarine landslides. *Reviews of geophysics*, 34 (1996) 33–59.

[16] W. H. Herschel and T. Bulkley. Measurement of consistency as applied to rubber-benzene solutions. *Proceedings of the American Society for Testing and Material*, 26 (1926) 621–633.

[17] A. J. Hogg and D. Pritchard. The effects of hydraulic resistance on dam-break and other shallow inertial flows. *J. Fluid Mech.*, 501 (2004) 179–212.

[18] X. Huang and M. Garcia. A Herschel-Bulkley model for mud flow down a slope. *J. Fluid Mech.*, 374 (1998) 305–333.

[19] H. E. Hupper. The propagation of two-dimensional and axisymmetric viscous gravity currents over a rigid horizontal surface. *J. Fluid Mech.*, 121 (1982) 43–58.

[20] I. Ionescu and M. Sofonea. *Functional and numerical methods in viscoplasticity*. Oxford university press, UK, 1993.

[21] D. Laigle and P. Coussot. Numerical modeling of mudflows. *J. Hydr. Engrg.*, 123 (1997) 617–623.

[22] K.-F. Liu and C. C. Mei. Approximation equations for the slow spreading of a thin Bingham plastic fluid. *Phys. Fluid A*, 2 (1990) 30–36.

[23] L.-H. Luu and Y. Forterre. Drop impact of yield-stress fluids. *J. Fluid Mech.*, 632 (2009) 301–327.

[24] G. P. Matson and A. J. Hogg. Two-dimensional dam break flows of Herschel-Bulkley fluids: The approach to the arrested state. *J. Non-Newtonian Fluid Mech.*, 142 (2007) 79–94.

[25] C. C. Mei and M. Yuhi. Slow flow of a Bingham fluid in a shallow channel of finite width. *J. Fluid Mech.*, 431 (2001) 135–159.

[26] K. D. Nikitin, M. A. Olshanskii, K. M. Terekhov, and Y. V. Vassilevski. Numerical method for the simulation of free surface flows of viscoplastic fluid in 3D. submitted, (2011).

[27] Y. S. Park and P. L.-F. Liu. Oscillatory pipe flows of a yield-stress fluid. *J. Fluid Mech.*, 658 (2010) 211–228.

[28] R. Perona. Bostwick degree and rheological properties: an up-to-date viewpoint. *Appl. Rheol.*, 15 (2005) 218–229.

[29] N. Roquet and P. Saramito. An adaptive finite element method for Bingham fluid flows around a cylinder. *Comput. Appl. Meth. Mech. Engrg.*, 192 (2003) 3317–3341.

[30] A. J. C. Barré de Saint-Venant. Théorie et équations générales du mouvement non permanent des eaux courantes. *Comptes Rendus des séances de l'Académie des Sciences, Paris, France, Séance 17*, 73 (1871) 147–154.
[31] P. Saramito. A new constitutive equation for elastoviscoplastic fluid flows. *J. Non Newtonian Fluid Mech.*, 145 (2007) 1–14.
[32] P. Saramito. A new elastoviscoplastic model based on the Herschel-Bulkley viscoplasticity. *J. Non Newtonian Fluid Mech.*, 158 (2009) 154–161.
[33] P. Saramito. *Efficient C++ finite element computing with Rheolef*. CNRS and LJK, 2011. http://www-ljk.imag.fr/membres/Pierre.Saramito/rheolef.
[34] P. Saramito and N. Roquet. An adaptive finite element method for viscoplastic fluid flows in pipes. *Comput. Meth. Applied Mech. Engng*, 190 (2001) 5391–5412.
[35] P. Saramito, C. Smutek, and B. Cordonnier. Numerical modeling of shallow non-newtonian flows: Part i. the 1d horizontal dam break problem revisited. *Int. J. Numer. Anal. Model. B*, to appear (2013).
[36] N. Villeneuve, D. R. Neuville, P. Boivin, P. Bachélery, and P. Richet. Magma crystallization and viscosity: a study of molten basalts from the Piton de la Fournaise volcano (La Réunion island). *Chemical Geology*, 256 (2008) 242–251.
[37] M. Yuhi and C. C. Mei. Slow spreading of fluid mud over a conical surface. *J. Fluid Mech.*, 519 (2004) 337–358.

[1] Lab. J. Kuntzmann – CNRS and Grenoble university, B.P. 53, 38041 Grenoble cedex 9, France

[2] Lab. géosciences – IPGP and La Réunion university, 15, av. René Cassin, CS 92003, 97744 Saint-Denis cedex 09, France

E-mail: noe.bernabeu@imag.fr and pierre.saramito@imag.fr and claude.smutek@univ-reunion.fr

URL: http://www-ljk.imag.fr/membres/Pierre.Saramito